Energy 88 (2015) 667–679

Contents lists available at ScienceDirect

Energy

journal homepage: www.elsevier.com/locate/energy

Solar fuel processing efficiency for ceria redox cycling using alternative oxygen partial pressure reduction methods

Meng Lin, Sophia Haussener*

Laboratory of Renewable Energy Science and Engineering, EPFL, Station 9, 1015 Lausanne, Switzerland

ARTICLE INFO

Article history:
Received 15 April 2015
Accepted 2 June 2015
Available online 8 July 2015

Keywords:
Solar fuels
Ceria redox cycling
Thermodynamics
Oxygen scavenger
Vacuum pump
Sweep gas

ABSTRACT

Solar-driven non-stoichiometric thermochemical redox cycling of ceria for the conversion of solar energy into fuels shows promise in achieving high solar-to-fuel efficiency. This efficiency is significantly affected by the operating conditions, e.g. redox temperatures, reduction and oxidation pressures, solar irradiation concentration, or heat recovery effectiveness. We present a thermodynamic analysis of five redox cycle designs to investigate the effects of working conditions on the fuel production. We focused on the influence of approaches to reduce the partial pressure of oxygen in the reduction step, namely by mechanical approaches (sweep gassing or vacuum pumping), chemical approaches (chemical scavenger), and combinations thereof. The results indicated that the sweep gas schemes work more efficient at non-isothermal than isothermal conditions, and efficient gas phase heat recovery and sweep gas recycling was important to ensure efficient fuel processing. The vacuum pump scheme achieved best efficiencies at isothermal conditions, and at non-isothermal conditions heat recovery was less essential. The use of oxygen scavengers combined with sweep gas and vacuum pump schemes further increased the system efficiency. The present work can be used to predict the performance of solar-driven non-stoichiometric redox cycles and further offers quantifiable guidelines for system design and operation.

1. Introduction

The direct solar-driven processing of fuels by the thermochemical splitting of H_2O and CO_2 into H_2 and CO, a mixture called syngas, is a promising pathway for renewable fuel synthesis. The syngas can further be converted into liquid fuels through a conventional Fischer-Tropsch process effectively providing a direct approach for liquid solar fuel processing [1,2]. This approach exhibits a small environmental impact, allows for direct solar energy storage, and permits using conventional energy distribution infrastructure [1–4]. Direct H_2O and CO_2 thermolysis is challenging since temperatures above 2700 K are needed for reasonable reaction convergence [5,6], and efficient high temperature gas separation of a (possible explosive) mixture is required. Thermochemical multi-step cycles have been proposed to circumvent these drawbacks [1,7–9]. Particularly two-step, non-volatile metal oxide-based cycles show promise in avoiding gas separation issues, working at lower temperatures compared to direct thermolysis, enabling relatively simple design and operation, and theoretically achieving high solar-to-fuel efficiencies [10–14]. Ceria non-stoichiometric redox cycling has attracted interest due to its non-volatile characteristics even at high operating temperature, fast kinetics causing high hydrogen generation rates [12,15,16], theoretical high solar-to-fuel efficiencies [13,14,17], and practical demonstration of reasonable efficiencies in working prototypes [18–21]. The two steps water and CO_2 splitting reactions through non-stoichiometric ceria cycling are given as ($\Delta\delta = \delta_{red} - \delta_{ox}$)

$$CeO_{2-\delta_{ox}} \rightarrow CeO_{2-\delta_{red}} + \frac{\Delta\delta}{2} O_2, \quad (1)$$

$$CeO_{2-\delta_{red}} + \Delta\delta H_2O \rightarrow CeO_{2-\delta_{ox}} + \Delta\delta H_2, \quad (2)$$

$$CeO_{2-\delta_{red}} + \Delta\delta CO_2 \rightarrow CeO_{2-\delta_{ox}} + \Delta\delta CO. \quad (3)$$

The endothermic reduction step, eq. (1), operates with reasonable conversion at temperatures ranging between 1400 K and 2100 K. The exothermic oxidation reactions, eqs. (2) and (3), favor lower temperatures in order to ensure a complete oxidation of ceria [12] with a typical temperature range of around 700 K–1100 K. The

* Corresponding author. Tel.: +41 21 693 3878.
E-mail address: sophia.haussener@epfl.ch (S. Haussener).

http://dx.doi.org/10.1016/j.energy.2015.06.006
0360-5442/

temperature difference between the two steps requires solid phase heat recovery in order to maintain a high solar-to-fuel efficiency [14], which is difficult to realize and increases the system complexity. Therefore, isothermal cycling has been proposed [16,22,23].

Thermodynamic evaluations of the performance of ceria redox cycling have been reported in Refs. [3,13,14,17,24]. Panlener et al. studied the reaction enthalpy of non-stoichiometric ceria in a large range of temperatures and pressures by thermogravimetric measurements [25]. Riess et al. [26] investigated the specific heat of ceria by an adiabatic temperature scanning calorimeter. Lapp et al. [15] performed a parametric thermodynamic analysis of a ceria-based cycling scheme using an ideal mixing model and sweep gassing to maintain a low oxygen concentration atmosphere for the reduction step. They found that effective solid phase heat recovery was crucial in achieving solar-to-fuel efficiencies above 10%. Bader et al. [13] demonstrated numerically that isothermal cycling of ceria was possible at the expense of reduced system performance. Sweep gas was used to reduce the oxygen partial pressure in the reduction chamber, gas phase heat recovery was assumed, and plug flow reactor models in counter flow arrangements were employed in both chambers. Gas phase heat recovery with effectiveness above 95.5% was required for solar-to-fuel efficiencies above 10%. The energy penalty introduced through the use of immense amounts of sweep gas pointed to the need for alternative methods to reduce the oxygen partial pressure during the reduction reaction. Ermanoski et al. [17] showed for the non-isothermal cycling of ceria using ideal mixing in both reaction chambers that the efficiency of the process could be increased by using vacuum pumping schemes for the reduction of the oxygen partial pressure. It is unclear whether this conclusion applies to isothermal operation and whether a further decrease of the oxygen partial pressure in the reduction chamber through non-mechanical methods is required for competitive solar-to-fuel efficiencies provided the use of solid–solid and gas–gas heat recovery components with realistic heat exchange effectiveness.

We developed a thermodynamic model for evaluating optimal operating conditions (system pressure, oxygen partial pressure, reduction temperature, oxidation temperature, heat recovery, and irradiation concentration ratio) for various system configurations of non-stoichiometric cycling of ceria using concentrated solar irradiation. Particularly, we focused on the reduction step and on the incorporation of alternative methods – mechanical and chemical – for reducing the oxygen partial pressure. The understanding of the influence of working conditions, component choices, and system configurations on system performance is required for the determination of the optimal operation conditions and design of practical system configurations for increased solar fuels processing efficiencies.

2. Thermodynamic model

2.1. Model development

Five thermochemical fuel production systems investigated are depicted in Fig. 1. They differed in their approaches to reduce the oxygen partial pressure in the reduction chamber, namely: three mechanical schemes using i) sweep gas (scheme a) [14,15], ii) vacuum pump (scheme b) [18], and iii) the combination thereof (scheme d); and two combined mechanical-chemical schemes using i) sweep gas and a chemical scavenger (scheme c), and ii) using the combination of sweep gas, vacuum pump, and a chemical scavenger (scheme e). All five systems used two continuously and simultaneously operating reaction chambers for the separated reduction and oxidation reactions. The systems incorporated two heat exchanges to recover the heat from the exhaust (sweep gas and products). Solid phase heat recovery was incorporated between the reduced and oxidized ceria streams.

In scheme (a) inert gas was used to sweep away the produced oxygen during the reduction and correspondingly maintaining a desired oxygen partial pressure at the entrance (process 3–4). The sweep gas flow and the ceria flow was considered in a counterflow arrangement [13], i.e. the pressure and temperature will stay constant while the concentration of oxygen and the δ of ceria vary only in axial direction. Compared to the ideal mixing flow design used in Refs. [15,18], the counterflow arrangement maximized the p_{O_2} in the sweep gas at the outlet of the reduction chamber and minimized the p_{O_2} at the outlet of the oxidation chamber, resulting in a reduced sweep gas demand and reactant input. The inert gas was preheated in a heat exchanger and further heated by concentrated solar energy to the reduction temperature, T_{red}, before entering the reduction chamber. The states 5 to 8 described a full, closed ceria cycle. The ceria was cooled to the oxidation temperature, T_{ox}, in the process 5–6 while rejecting Q_{ceria} (not needed for isothermal operation), and isothermally reacted with the oxidizing agents (H_2O, CO_2) in the oxidation chamber during the process 6–7. Finally, the ceria temperature was heated to T_{red} (process 7–8) and then isothermally reduced in the reduction chamber (process 8–5). The oxidizer was preheated in the heat exchanger by effluent and further heated to T_{ox} by concentrated solar energy (process 10–11). Since the oxidation reaction was an exothermic process, the energy needed to heat the oxidizer from T_{10} to T_{11} may be less than the heat released by the reaction and hence a heat exchanger was used for further exhaust cooling after heat recovery (process 13–14).

The processes of scheme (b) were similar to the processes in scheme (a) concerning the oxidation process and the ceria cycling process. However, the oxygen generated in the reduction chamber was not swept away by inert gas. Instead a vacuum pump was employed continuously removing the produced oxygen during the reduction and maintaining a desired oxygen partial pressure in the chamber.

In scheme (c), sweep gassing was combined with a chemical oxygen scavenger (process 1′–2′) in which the oxygen in the sweep gas is reacted with an active metal (e.g. magnesium) to further reduce the oxygen partial pressure. Magnesium has been reported to be an alloying element in metals industries acting an important chemical oxygen scavenger which is widely used is large scale metal alloy production [27,28]. Magnesium oxide can be recycled through various thermochemical and electrochemical processes which are commonly used for industrial magnesium production [29].

Scheme (d) was a combination of both mechanical approaches, namely sweep gassing and vacuum pump. Scheme (e) combined scheme (d) with the chemical scavenger.

Additional assumptions used in the model were: *i*) the system was evaluated at steady state, *ii.a*) for scheme (a), counterflow arrangement was assumed for both reduction and oxidation chamber, *ii.b*) for scheme (b), counterflow arrangement was assumed in the oxidation chamber and the oxygen was uniformly distributed in the reduction chamber, *iii*) gases were modeled as ideal gases, and *iv*) temperatures of the reactants in the reduction and oxidation chambers were considered constant and uniform.

Additionally, we used ideal mixing models for the reduction and oxidation chambers to account for a less favorable reaction chamber design configuration. The ideal mixing model considered the equilibrium p_{O_2} that was created by the water at T_{ox}, influencing the non-stoichiometry at oxidation. In this case, the p_{O_2} in the oxidation chamber was determined by optimizing it for largest cycle efficiency while ensuring it was smaller than p_{O_2} of water dissociation at T_{ox}.

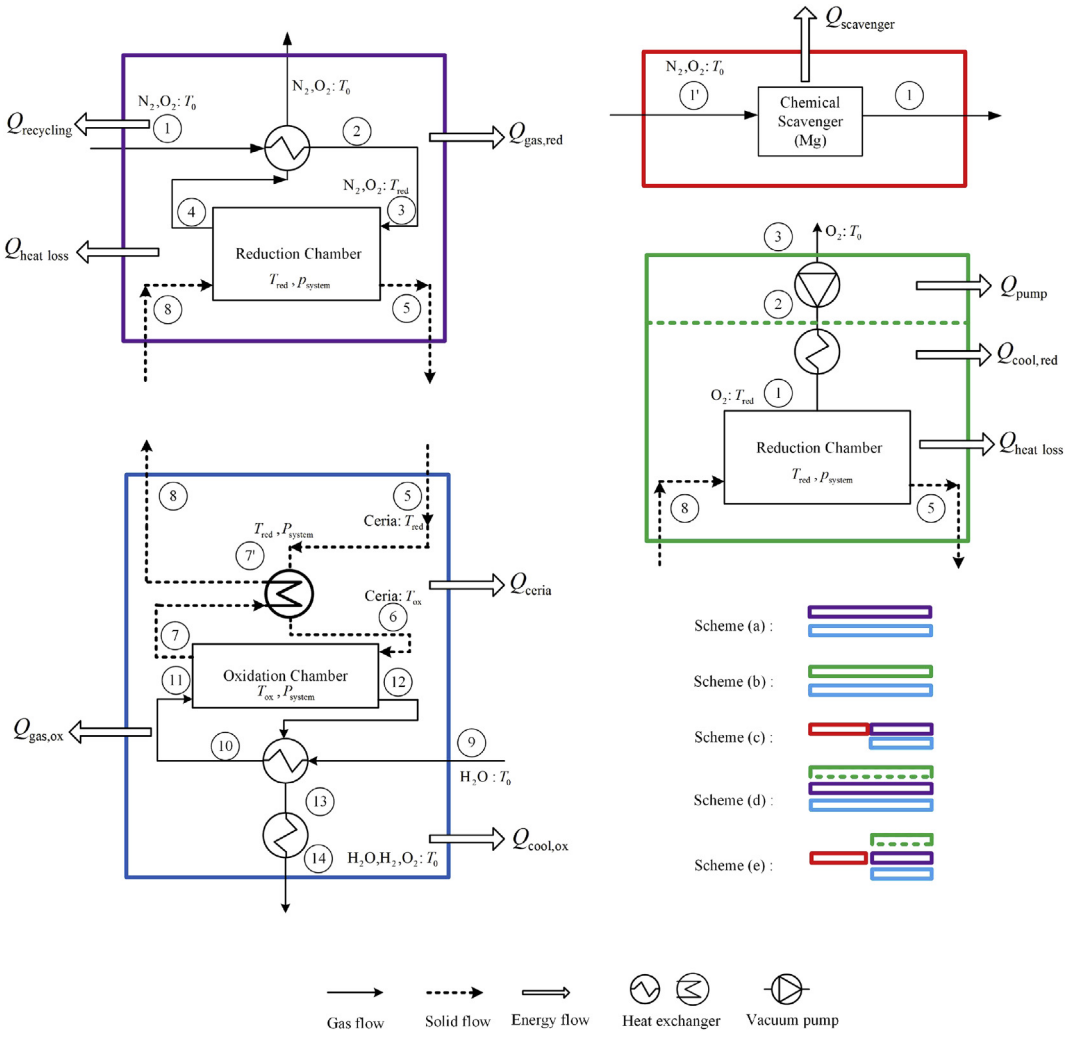

Fig. 1. Schematic of the five ceria-based thermochemical cycling schemes modeled (a to e), which are combinations of four different sub-components: oxidation chamber and auxiliaries (blue), reduction chamber and sweep gas connections (purple), chemical scavenger (red), and reduction chamber and vacuum pump (green). The five schemes differ in the methods used for the oxygen partial pressure reduction in the reduction chamber, namely: using inert sweep gas, a vacuum pump, a chemical scavenger, or combinations thereof.

The steady state energy balance for the modeled system was given by

$$\dot{Q}_{solar} = \dot{Q}_{heat\ loss} + \dot{Q}_{react} + \dot{Q}_{gas,red} + \dot{Q}_{gas,ox} + \dot{Q}_{cool,ox} + \dot{Q}_{cool,red} + \dot{Q}_{ceria} + \dot{Q}_{pump} + \dot{Q}_{recycling} + \dot{Q}_{scavenger} \quad (4)$$

$\dot{Q}_{solar}$ was the solar energy incident on a blackbody receiver with a certain aperture area for concentrated solar irradiation ($\dot{Q}_{solar} = A_{ap}CI$). Note that the last three terms on the right hand side ($\dot{Q}_{pump}, \dot{Q}_{recycling}, \dot{Q}_{scavenger}$) are not all concurrently required for all schemes, as detailed below. The heat losses accounted for the radiation heat loss from the aperture, and conduction and convection losses through the cavity walls. The latter were assumed to be a constant fraction, f, of the total solar energy captured by the cavity and assumed 20% according to experimental observations [30]. Hence, the heat losses were given by

$$\dot{Q}_{heat\ loss} = \dot{Q}_{rad} + f\left(\dot{Q}_{solar} - \dot{Q}_{rad}\right) = (1-f)A_{ap}\sigma T_{red}^4 + f\dot{Q}_{solar}. \quad (5)$$

The power utilized for the chemical reaction was the sum of the chemical reactions in the reduction and oxidation chambers,

$$\dot{Q}_{react} = \dot{Q}_{react,ox} + \dot{Q}_{react,red} = \dot{n}_{H_2}\Delta h_{H_2O,react}(T_{ox}), \quad (6)$$

where $\dot{Q}_{react,red} = -\dot{Q}_{react,ox} = \dot{n}_{ceria}/2\int_{\delta_{ox}}^{\delta_{red}} \Delta h_{O_2}(\delta)\mathrm{d}\delta$. We focused our investigations on the splitting of water. Nevertheless, the splitting of CO_2 or a combination of water and CO_2 can be studied analogously and selected results are presented in the supporting information.

In scheme (a), the sweep gas was preheated in a heat exchanger (with recovery effectiveness, ε_g) by heat of the effluent,

$$\dot{Q}_{gas,red} = (1-\varepsilon_g)\dot{n}_{N_2,1}\left[h_{N_2}(T_{red}) - h_{N_2}(T_0)\right] + (1-\varepsilon_g)\dot{n}_{O_2,1}\left[h_{O_2}(T_{red}) - h_{O_2}(T_0)\right], \quad (7)$$

before entering the reduction chamber where the final T_{red} was achieved through part of the solar irradiation. $\dot{n}_{O_2,1}$ was the molar flow of oxygen in the inert gas before entering the reduction chamber.

$\dot{Q}_{gas,red} = 0$ in scheme (b) since no sweep gas was introduced. However, the oxygen produced in the ceria reduction process was continuously pumped out by a vacuum pump and, for practical reasons, has to be cooled before entering the pump. The energy loss due to cooling is calculated as

$$\dot{Q}_{cool,red} = (\dot{n}_{O_2,4} - \dot{n}_{O_2,1})\left[h_{O_2}(T_{red}) - h_{O_2}(T_0)\right]. \quad (8)$$

Similarly, the energy required for the heating of the oxidizer was given as

$$\dot{Q}_{gas,ox} = (\dot{n}_{H_2O,9} - \varepsilon_g \dot{n}_{H_2O,12})\left[h_{H_2O}(T_{ox}) - h_{H_2O}(T_0)\right] - \varepsilon_g \dot{n}_{H_2,12}\left[h_{H_2}(T_{ox}) - h_{H_2}(T_0)\right] - \varepsilon_g \dot{n}_{O_2,12}\left[h_{O_2}(T_{ox}) - h_{O_2}(T_0)\right]. \quad (9)$$

The oxidation reaction was slightly endothermic which can lead to excessive heat in the oxidation chamber. In this case cooling was considered in the energy balance by

$$\dot{Q}_{cool,ox} = \dot{Q}_{react,ox} - \dot{Q}_{gas,ox}. \quad (10)$$

For non-isothermal operation, ceria needed to be heated from the oxidation to the reduction temperature,

$$\dot{Q}_{ceria} = \dot{n}_{ceria} \int_{T_{ox}}^{T_{red}} c_{p,ceria} dT. \quad (11)$$

Similarly, the ceria needed to be cooled from the reduction to the oxidation temperature when exiting the reduction chamber. Potentially, the rejected heat during this cooling step can be partially recovered in a solid–solid heat exchanger (with a effectiveness, ε_s) in order to minimize the required $\dot{Q}_{ceria}$ for the solid heating step (eq. (11)).

The pumping work for the cycling of the gas and solid reactants and products in both reaction chambers and through the piping was neglected in all schemes. The pumping work required in scheme (b) to remove the generated oxygen in the reduction process was calculated by

$$\dot{Q}_{pump} = \frac{W_{pump}}{\eta_t \eta_{pump}} = \frac{\dot{n}_{O_2,1} R T_0}{\eta_t \eta_{pump}} \ln \frac{p_0}{p_{O_2,1}}, \quad (12)$$

where W_{pump} was the pumping work for moving the oxygen stream out of reduction chamber, η_t was the heat-to-electricity efficiency, η_{pump} was the electricity-to-pumping work efficiency, p_0 was the ambient pressure, and p_{O_2} was the partial pressure of oxygen in the reduction chamber.

The energy for recycling the sweep gas, $\dot{Q}_{recycling}$, occupied less than 1% of the total solar energy input [13] and was neglected in the current study. The recycling energy of the chemical scavenger is given by

$$\dot{Q}_{scavenger} = \frac{\dot{n}_{N_2,1'}\left(p_{O_2,2'} - p_{O_2,1'}\right)}{p_0} \dot{Q}_{Mg,pr}, \quad (13)$$

where the $\dot{Q}_{Mg,pr}$ was the total energy need to produce 1 mol of magnesium, which was obtained from industrial databases [31].

The molar flow rates of all streams at each state were obtained by solving the mass balance in both chambers considering chemical equilibrium, counterflow or ideal mixing arrangement, respectively, and a two-step oxidation reaction including the water thermolysis and oxidation of reduced ceria by oxygen [13]. δ_{red} was determined by the p_{O_2} and T_{red} at the inlet of the reduction chamber, and δ_{ox} was obtained according to the p_{O_2} and T_{ox} at the inlet of the oxidation chamber. p_{O_2} at the inlet of the oxidation chamber only depended on T_{ox} and hence also δ_{ox} was only a function of T_{ox}.

The non-stoichiometry coefficient, δ, for the undoped ceria reduction and oxidation reaction under various conditions was determined using the experimental data of Panlener et al. [25], in which experiments for oxygen partial pressures and temperatures ranging from 10^{-22} atm to 10^{-2} atm and 1023 K–1774 K, respectively, with δ varying from 0.00107 to 0.27 were performed. The values of δ were calculated for given temperatures and p_{O_2} by,

$$\Delta g_{O_2}(\delta, T) = \Delta h_{O_2}(\delta) - T\Delta s_{O_2}(\delta) = RT \ln \frac{p_{O_2}}{p_0}. \quad (14)$$

The specific heat of nonstoichiometric ceria was estimated by the specific heat of cerium dioxide without considering the impact of phase transformations [26].

2.2. Definitions

Three performance indicators were used in this study: *i*) the solar-to-fuel efficiency, *ii*) water utilization factor, and *iii*) hydrogen productivity. The solar-to-fuel efficiency, η, was defined as

$$\eta = \frac{\dot{n}_{H_2,12} HHV_{H_2}}{\dot{Q}_{solar}}. \quad (15)$$

The water utilization factor, f_w, was the ratio between the amount of hydrogen produced and the total water input into the oxidation chamber,

$$f_w = \frac{\dot{n}_{H_2,12}}{\dot{n}_{H_2O,9}}. \quad (16)$$

f_w indicated the efficiency of input water usage which can be maximized when the water input needs to be minimized (e.g. when water resources are scarce). Note that $\dot{n}_{H_2O,9}$ was determined by the reaction's thermodynamic equilibrium at state points 11 and 12, which was not randomly chosen but requires the oxygen partial pressure at the outlet to match $p_{O_2,12}$.

The hydrogen productivity, χ_{H_2}, was the ratio between the production rate of hydrogen at 1 kW solar power input and the solid metal oxide rate required for the cycling,

$$\chi_{H_2} = \frac{\dot{n}_{H_2,12}}{\dot{n}_{ceria,5}}. \quad (17)$$

It quantified the efficiency of metal oxide utilization and indicated the amount of ceria which has to be moved in such a system.

All the aforementioned definitions are analogous when evaluating the CO_2 dissociation for the CO production.

3. Results

3.1. Operational feasibility for ceria-based fuel processing cycles

The operational feasibility and limitation of the proposed ceria based thermochemical cycle schemes were given by two conditions: *i*) $\delta_{red} > \delta_{ox}$ to ensure a net fuel production, and *ii*) $p_{O_2,1} \le p_{O_2,4} \le p_{system}$ (not required for scheme (b)). The combinations of T_{red}, $\Delta T = T_{red} - T_{ox}$, and $p_{O_2,4}$ for which condition *i*) is met are depicted in Fig. 2a. The combinations for which condition *ii*) is met are depicted in Fig. 2b.

For isothermal operation ($\Delta T = 0$ and $p_{O_2,4} = p_{O_2,11}$), condition *ii*) was fulfilled for all T_{red} investigated ($1400 < T_{red} < 2100$ K) at a

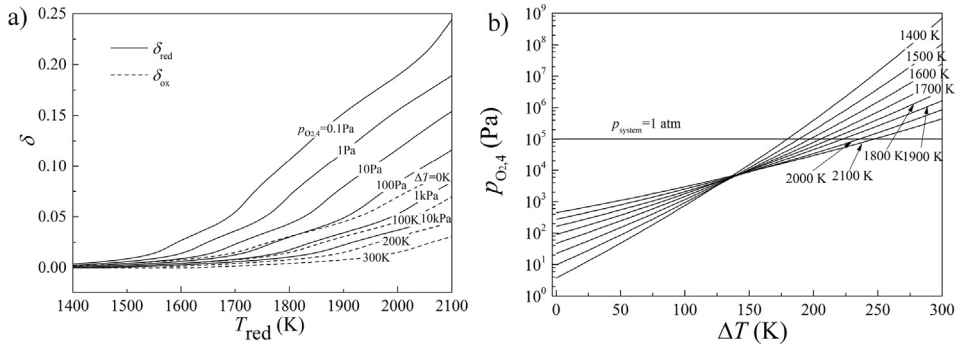

Fig. 2. Feasibility of ceria-based thermochemical cycling under various operation conditions: a) the non-stoichiometric coefficient of ceria at various temperatures and $p_{O_2,4}$, and b) $p_{O_2,4}$ as a function of ΔT for various T_{red}.

system pressures of 1 atm. A system pressure as low as 6 mbar could be tolerated. At $p_{system} = 1$ atm, isothermal operation was feasible once the condition $\delta_{red} > \delta_{ox}$ is met, which required $p_{O_2,4} < 100$Pa for $T_{red} > 1800$ K (see Fig. 2a). The higher $p_{O_2,4}$ the higher T_{red} required for a positive net fuel production. The maximum $p_{O_2,1}$ that was possible for isothermal operation was about 460 Pa for $T_{red} > 1400$ K. For non-isothermal operation ($\Delta T \neq 0$), the largest possible ΔT was about 250 K for $p_{system} = 1$ atm and $T_{red} = 2100$ K. The increase in ΔT from 0 K (isothermal) to 300 K enlarged the range of feasible operational conditions that still ensured $\delta_{red} > \delta_{ox}$ (see Fig. 2a), but also increased$p_{O_2,4}$, eventually requiring an increased system pressure for feasibility. An increase in p_{system} increased the range of possible operational conditions, i.e. allows for larger ΔT.

3.2. Effects of temperature swing and oxygen partial pressure

The T_{red}, T_{ox} (or ΔT), $p_{O_2,1}$, and p_{system} were the most significant operational parameters. Large T_{red} led to increased heat losses (see eq. (5)), but increased δ_{red}, which increased the potential to produce hydrogen. Large ΔT resulted in increased hydrogen production due to the decreased δ_{ox}, while introducing an increased solid phase heat loss (see eq. (11)) if solid heat recovery was not practical or efficient. A smaller $p_{O_2,1}$ required higher flow rates of sweep gas and correspondingly more energy to heat up the sweep gas, or more pumping work for the vacuum pump. Nevertheless, small $p_{O_2,1}$ increased δ_{red} and provided a larger hydrogen production potential. A reference case was defined (see Table 1) for the subsequent optimization. Particularly, we optimized ΔT for maximum solar-to-fuel efficiency at a particular combination of T_{red} and $p_{O_2,1}$.

Fig. 3 shows the calculated largest possible efficiencies for various combinations of T_{red} and $p_{O_2,1}$, indicating the corresponding optimized ΔT, for scheme (a) and (b). This efficiency is called optimal efficiency. Additionally, the efficiency for the same T_{red} and $p_{O_2,red}$ combinations at isothermal operation ($\Delta T = 0$) are shown. The corresponding energy distribution is depicted in Figs. 4 and 5 for scheme (a) and (b), respectively.

For scheme (a), the best performing cases for all combinations of T_{red} and $p_{O_2,1}$ operated non-isothermally ($\Delta T > 0$). The optimal η increased with increasing T_{red} due to decreasing $\dot{Q}_{gas,ox}$, and increasing $\Delta\delta$, until $\dot{Q}_{heat\ loss}$ started to dominate the energy balance resulting in a decreasing η (see Fig. 4d). The impact of T_{red} on η at isothermal operation is illustrated in Fig. 4a and revealed that initially $\dot{Q}_{gas,red}$, $\dot{Q}_{gas,ox}$, and $\dot{Q}_{heat\ loss}$ were dominating. The latter was continuously increasing with increasing T_{red}, while the former two were monotonically decreasing at a faster rate.

Compared to the isothermal operation, a small ΔT led to a significantly higher η, i.e. the solar-to-fuel efficiency for $p_{O_2,1} = 0.1$ Pa, $T_{red} = 1800$ K was 11% for isothermal operation and 31% at $\Delta T = 135$ K. The increase of ΔT, while increasing $\dot{Q}_{solid}$, resulted in a significant drop of δ_{ox} which results in an increase in the hydrogen production due to the increasing $\Delta\delta$ (see Fig. 4c). The amount of inert sweep gas required decreased with increasing ΔT due to significantly increasing $p_{O_2,4}$ and consequently reduced sweep gas amount hence reduced $\dot{Q}_{gas,red}$. At $\Delta T > 150$, $\dot{Q}_{cool,ox}$ appeared and increased with ΔT reducing the efficiency gain brought by the decrease of $\dot{Q}_{gas,red}$ (Fig. 4c). This indicates that a temperature swing will largely increase the system performance compared to isothermal operation and there exist an optimal ΔT for the best performance which is in the rage of 125 K.

Lowering $p_{O_2,1}$ always causes an increase in η for a given T_{red} due to the significant increase in δ_{red}. The T_{red} for optimal η moved to higher values as $p_{O_2,1}$ increased while requiring larger ΔT (see Fig. 3a). For very large $p_{O_2,1}$, the low $\Delta\delta$ is the reason for low efficiencies. This can be alleviated by operating at larger ΔT.

Table 1
Reference case parameters used for the comparison of the five different models of the ceria cycling.

Parameter	Value	Unit
Direct normal irradiance, I	1	kW/m^2
Solar concentration ratio, C	3000	
System pressure, p_{system}	1	atm
Heat loss factor, f	0.2 [31]	
Heat-to-electricity efficiency, η_t	0.4	
Electricity-to-pumping efficiency, η_{pump}	0.4 [32]	
Reduction temperature, T_{red}	1400–2100	K
Temperature swing, ΔT	0–300	K
Oxygen partial pressure in the sweep gas for scheme (a), $p_{O_2,1}$	1.1–20,000	Pa
Oxygen absolute pressure in the reduction chamber for scheme (b), $p_{O_2,1}$	1.1–20,000	Pa
Ambient temperature, T_0	298	K
Heat recovery effectiveness for gases, ε_g	0.955 [34]	
Heat recovery effectiveness for solid, ε_s	0	

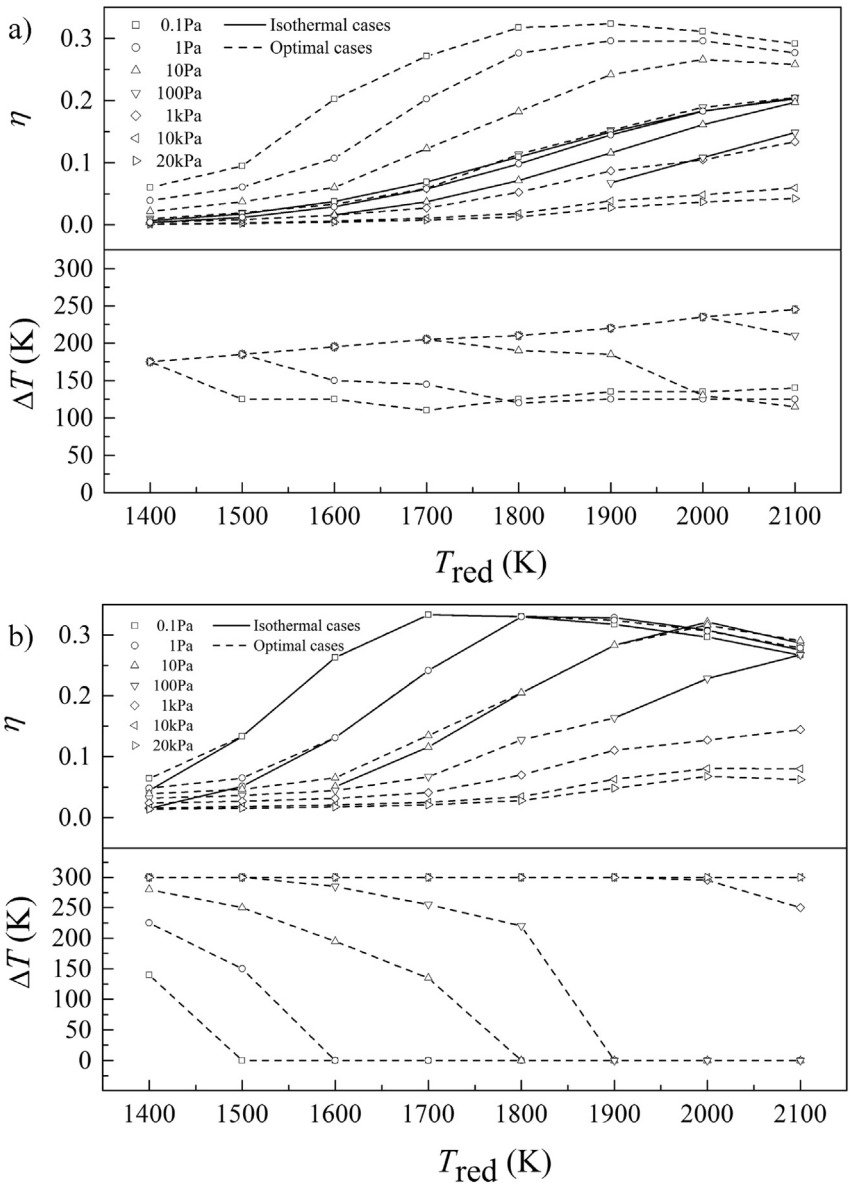

Fig. 3. Optimal η (dotted lines) and corresponding ΔT for various T_{red} and $p_{O_2,1}$ combinations for a) scheme (a), and b) scheme (b). The solid lines indicate the efficiency at corresponding T_{red} and $p_{O_2,1}$ for isothermal operation ($\Delta T = 0$).

Small δ_{red} resulted at low T_{red} and large $p_{O_2,1}$. These combinations required a large ΔT (often unfeasible, see Fig. 2b) for reasonable efficiencies and comparatively higher $\Delta\delta$. As T_{red} increased, δ_{red} increased gradually leading to a dominating $\dot{Q}_{ceria}$ and corresponding required a decrease in ΔT, for optimal η (see Fig. 3a). For $p_{O_2,1} > 100$ Pa, ΔT was always restricted by the feasibility conditions and consequently the activity of the reduction of ceria is hindered at large $p_{O_2,1}$. A slight increase in ΔT was detected for $p_{O_2,1} = 0.1$ Pa and 1 Pa at 1700 K and 1800 K, respectively. This is due to the appearance of $\dot{Q}_{cool,ox}$ at high temperatures which can partly be compensated by a larger ΔT.

The results for scheme (b) revealed that the optimal η under various given T_{red} and $p_{O_2,1}$ tend to work at lower ΔT which favored isothermal operation compared to scheme (a). This trend was especially pronounced at higher temperatures ($T_{red} \geq 1800$ K). This was caused by the increase in $\Delta\delta$ and decrease in $\dot{Q}_{pump}$ and $\dot{Q}_{gas,ox}$ with increasing ΔT and T_{red}, which was overcompensated by the increasing $\dot{Q}_{cool,ox}$ and $\dot{Q}_{ceria}$ (see Fig. 5c and dc).

Similar trends in the optimal η (i.e. at non-isothermal conditions, $\Delta T \neq 0$) were observed for scheme (b) and scheme (a). Increasing $p_{O_2,1}$ led to a significant reduction in η for the whole range of $p_{O_2,1}$ studied (0.1 Pa–20000 Pa) for $T_{red} < 1700$ K. For $T_{red} > 1700$, $p_{O_2,1} > 0.1$ Pa showed larger optimal η than $p_{O_2,1} = 0.1$ Pa ($\eta = 30\%$ for $p_{O_2,1} = 0.1$ Pa, and $\eta = 31\%$ for $p_{O_2,1} = 1$ Pa at $T_{red} = 2000$ K) due to the decrease in $\dot{Q}_{pump}$, $\dot{Q}_{cool,ox}$, and $\dot{Q}_{cool,red}$ at high T_{red} (Fig. 5b and 5d) which overruled the decrease of $\Delta\delta$.

The efficiencies of the system for CO_2 splitting (eqs. (1) and (3)) showed similar trends as the ones described for water splitting in schemes (a) and (b) with generally higher efficiencies due to larger equilibrium constants for the oxidation reaction in the CO_2 splitting system. The efficiency variations for solar thermochemical ceria-based CO_2 splitting for varying T_{red}, $p_{O_2,1}$, and ΔT are shown in Figs. S1 and S2.

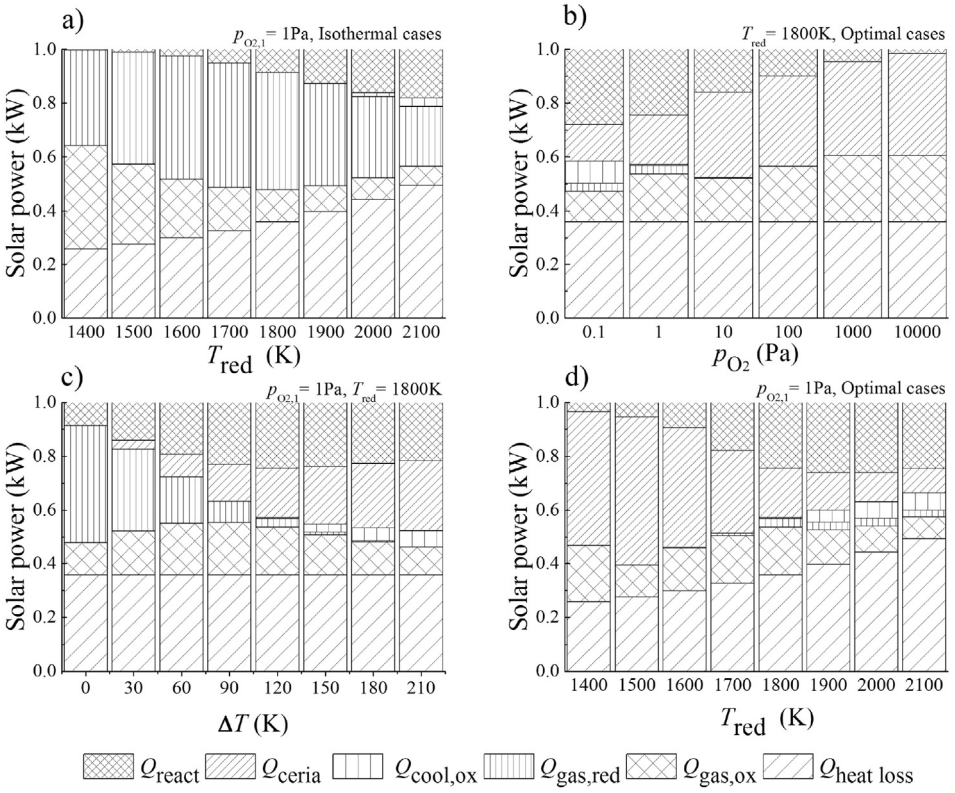

Fig. 4. Energy balance for scheme (a) at 1 kW solar power input under various working conditions: a) isothermal cases at $p_{O_2,1} = 1$ Pa for varying T_{red}, b) optimal cases at $T_{red} = 1800$ K for varying $p_{O_2,1}$, c) cases at $p_{O_2,1} = 1$ Pa and $T_{red} = 1800$ K for varying ΔT, and d) optimal cases at $p_{O_2,1} = 1$ Pa for varying T_{red}.

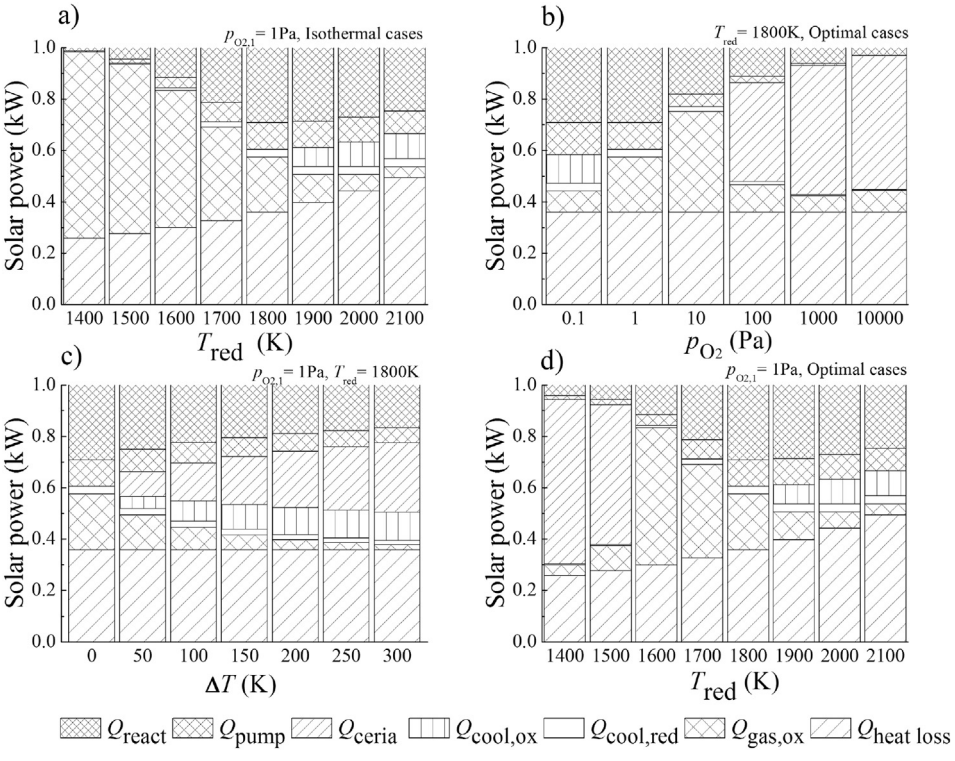

Fig. 5. Energy balance for scheme (b) at 1 kW solar power input under various working conditions: a) isothermal cases at $p_{O_2,1} = 1$ Pa for varying T_{red}, b) optimal cases at $T_{red} = 1800$ K for varying $p_{O_2,1}$, c) cases at $p_{O_2,1} = 1$ Pa and $T_{red} = 1800$ K for varying ΔT, and d) optimal cases at $p_{O_2,1} = 1$ Pa for varying T_{red}.

3.3. Hydrogen productivity

In addition to an optimized solar-to-fuel efficiency, the hydrogen productivity should be maximized in order to minimize the amount of metal oxide which needs to be cycled (pumping requirements), bought and refilled (economic investment), and mined and recycled (sustainability issue).

χ_{H_2} is shown in Fig. 6 exemplary for a practical T_{red} of 1800 K χ_{H_2} increased with increasing ΔT and decreasing $p_{O_2,1}$. The two zones shown in Fig. 6 distinguished the accessibility of ΔT for scheme (a) and scheme (b) as discussed in section 3.1. For scheme (a), the ΔT was limited by $p_{O_2,4}$ and the operation is only possible in zone 1. For scheme (b), the operation was not confined by $p_{O_2,4}$ and hence zone 1 and zone 2 were accessible. The increase in ΔT effected a lower δ_{ox} resulting in a larger $\Delta\delta$ and correspondingly larger χ_{H_2}. Generally, the optimal efficiencies of scheme (a) were situated at $\Delta T > 0$ and correspondingly higher hydrogen productivities were achieved (indicated by the hollow dots in Fig. 6) compared to the optimal efficiencies of scheme (b), which usually were isothermal or at low ΔT (for $p_{O_2,1} < 100$ Pa). For $p_{O_2,1} \geq 100$ Pa, large χ_{H_2} were achieved in scheme (b), however, η was significantly limited by low $\Delta\delta$. Generally, operating at optimal efficiencies and low $p_{O_2,1}$ required more ceria per produced hydrogen for vacuum pumping approach (scheme (b)) compared to sweep gassing (scheme (a)). Since the sensitivity of the efficiency with the variation of ΔT for scheme (b) at 1800 K is small (see Fig. 5c), it is possible to optimize the operational conditions for scheme (b) by operating at a small ΔT (within 150 K) to achieve both high solar-to-fuel efficiency (28% at $T_{red} = 1800$ K, $p_{O_2,1} = 1$ Pa, and $\Delta T = 120$ K) and comparatively larger hydrogen productivity.

3.4. Water utilization factor

Fig. 7 exemplary shows f_w for schemes (a) and (b) at $T_{red} = 1800$ K for varying $p_{O_2,1}$ and ΔT. Generally, lower $p_{O_2,1}$ and higher ΔT led to larger f_w. δ_{red} increases and correspondingly $p_{O_2,12}$ decreased with decreasing $p_{O_2,1}$ hence requiring a smaller water input. The enhancement in f_w with increasing ΔT was more pronounced at lower $p_{O_2,1}$ in accordance with a larger $\Delta\delta$ at these conditions and more efficient water use. The increase in f_w with increasing ΔT resulted from the lower $p_{O_2,1}$ at higher ΔT.

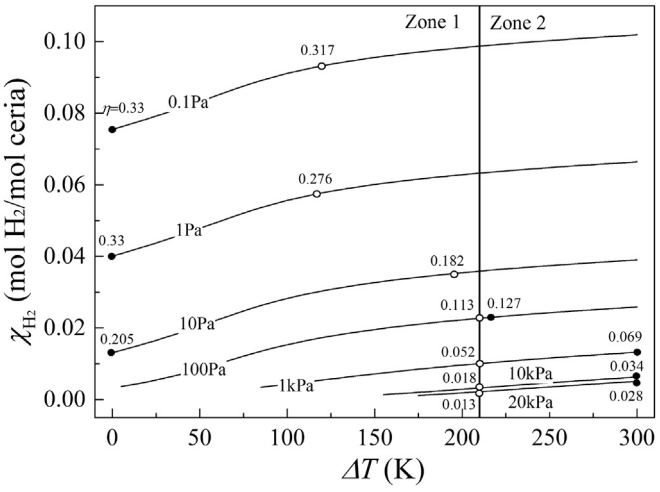

Fig. 6. H_2 productivity as a function of ΔT for different $p_{O_2,1}$ at $T_{red} = 1800$ K for scheme (a) (Zone 1) and scheme (b) (Zones 1 and 2). Dots indicate the optimal efficiency at the corresponding conditions (ΔT and $p_{O_2,1}$) for scheme (a) (hollow dots) and scheme (b) (filled dots).

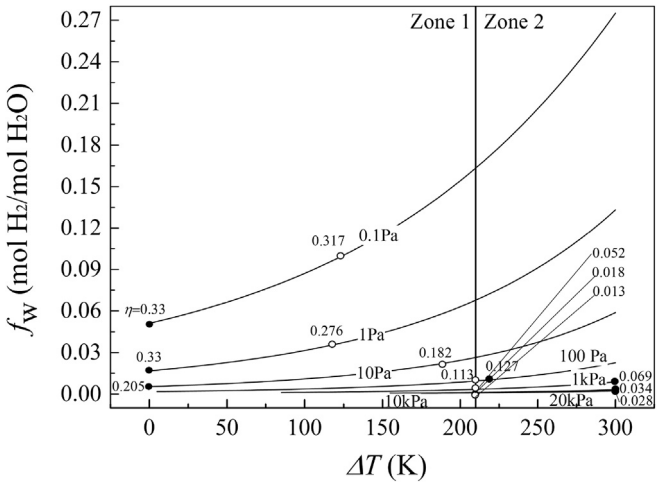

Fig. 7. f_w as a function of ΔT for different $p_{O_2,1}$ at $T_{red} = 1800$ K for scheme (a) (Zone 1) and scheme (b) (Zones 1 and 2). Dots indicate the optimal efficiency at the corresponding conditions (ΔT and $p_{O_2,1}$) for scheme (a) (hollow dots) and scheme (b) (filled dots).

Similar as for χ_{H_2}, scheme (a) worked at higher efficiency when $\Delta T \neq 0$, which in turn resulted in larger f_w. For scheme (b), isothermal operation led to higher η while unfavorably reduced the hydrogen productivity and f_w, which increased the consumption of input materials (water and ceria).

3.5. Pump efficiency

The electricity-to-pump efficiency, η_{pump}, for scheme (b) was assumed constant (40%) but practical vacuum pumps (rotary vane, piston, scroll, or roots pumps) show non-constant efficiencies changing with working conditions (pressure and flow rate). The effect of the decreasing pump efficiency with decreasing $p_{O_2,1}$ is depicted in Fig. 8a for a turbo molecular vacuum pump system of Pfeiffer Vacuum with a pump efficiency estimated as [32],

$$\eta_{pump} = 0.4 + 0.07 \log \frac{p_{O_2,1}}{p_0}. \quad (18)$$

The optimal η was significant affected by η_{pump} at low $p_{O_2,1}$ due to the decrease in η_{pump} with decreasing $p_{O_2,1}$. The increased power required for reducing the oxygen partial pressure is offset through an increase in T_{red}.

The optimal η was achieved at isothermal operation at low $p_{O_2,1}$, supporting the previous conclusion that vacuum pumping is the method of choice to lower the $p_{O_2,1}$ at isothermal conditions. The effect of η_{pump} on the optimal η under different $p_{O_2,1}$ is depicted in Fig. 8b and exhibits that η_{pump} of 40% is required to overcome the limitations posed by the pumping work. Further increase in η_{pump} showed no significant increase in the solar-to-fuel efficiency. These investigations provide guidelines for the choice of the vacuum pump technology and quality.

3.6. Heat recovery effectiveness

3.6.1. Gas phase heat recovery effectiveness

Gas phase heat recovery is crucial in dictating a large η [13]. As depicted in Fig. 9a, the larger ε_g the larger η at isothermal condition for scheme (a). ε_g as high as 0.975 was required for $\eta > 10\%$ at $T_{red} = 1700$ K. The increase in η was more pronounced at larger ε_g and with increasing T_{red}, further suggesting that the requirements on the high temperature heat exchanger manufacturing and maintenance were stringent when considering isothermal

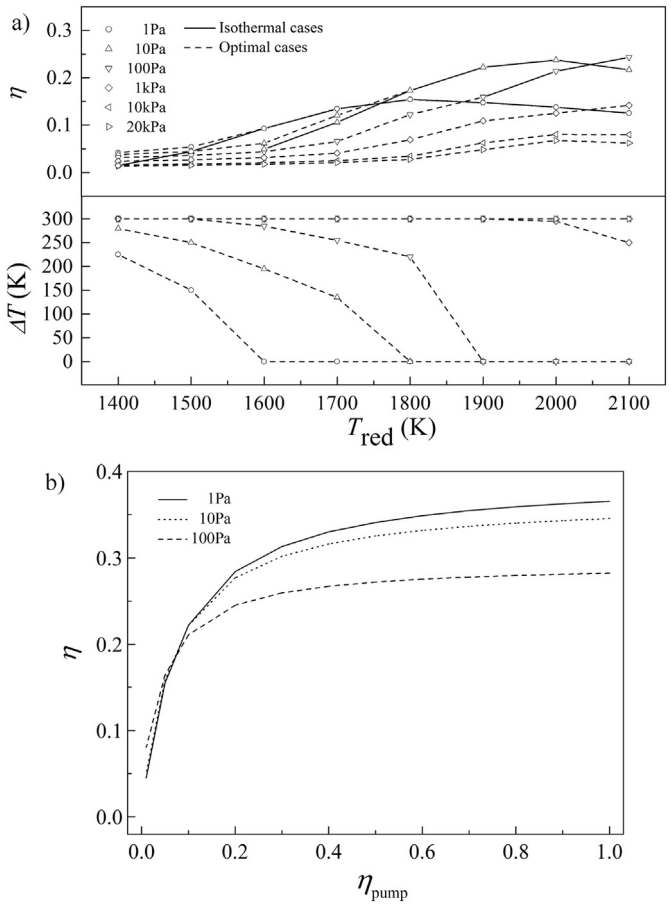

Fig. 8. a) Optimal η for various T_{red} and $p_{O_2,1}$ for scheme (b) with changing η_{pump} according to eq. (18), and b) optimal η as a function of η_{pump} for three different $p_{O_2,1}$ (1 Pa, 10 Pa, and 100 Pa).

operation. The requirements on the heat exchanger can be relaxed through the use of a temperature swing as depicted in Fig. 9b. At $\varepsilon_g < 0.9$, the maximum η appeared at the largest possible ΔT, where ΔT was limited by the operational feasibility (see section 3.1). For $\varepsilon_g > 0.9$, the highest solar-to-fuel efficiency was observed at an optimized ΔT which maximized the $\Delta\delta$ while limiting $\dot{Q}_{ceria}$.

For scheme (b), increasing ε_g at isothermal operation led to a significant increase in η at lower T_{red} ($T_{red} < 1800$ K), while a less pronounced effect was exhibited at high T_{red} (see Fig. 9c) due to the exhibited dominance of $\dot{Q}_{heat\ loss}$ (see Fig. 5). Compared to scheme (a), the requirements on the heat exchanger were less stringent and already a ε_g of 0.85 was sufficient to reach $\eta > 10\%$ at $T_{red} = 1700$ K. The requirements on the heat exchanger can be further relaxed when operating non-isothermally, as depicted in Fig. 9d. At $\Delta T = 300$ K, η was equal for $\varepsilon_g = 0.5$ and 0.975. An optimal ΔT for maximized optimal efficiency was observed for $\varepsilon_g < 0.9$. This resulted from a tradeoff between decreasing $\dot{Q}_{gas,ox}$ and increasing $\dot{Q}_{ceria}$ and $\dot{Q}_{cool,ox}$ as ΔT increased. For $\varepsilon_g > 0.9$, the decrease in $\dot{Q}_{gas,ox}$ with increasing ΔT was not observable as $\dot{Q}_{ceria}$ and $\dot{Q}_{cool,ox}$ dominated the losses already at $\Delta T = 0$ and further increased with increasing ΔT. Consequently, for $\varepsilon_g > 0.9$, isothermal operation resulted in the best performing solar-to-fuel efficiency. This feature of scheme (b) indicates that $\varepsilon_g \geq 0.9$ is required to ensure that isothermal operation results in the highest solar-to-fuel efficiency for a certain T_{red} and $p_{O_2,1}$ combination. Nevertheless, the introduction of a small ΔT can significantly reduce the requirements on the heat exchanger at a reasonable penalty in solar-to-fuel efficiency, *i.e.* introducing a ΔT of 50 K reduced the solar-to-fuel efficiency by 5.2% at $\varepsilon_g = 0.975$.

For $\varepsilon_g = 1$, the solar-to-fuel efficiency solely decreased with increasing T_{red} for isothermal operation of schemes (a) and (b), e.g. the efficiency of scheme (a) decreased from 50.8% to 36.4% as T_{red} increased from 1400 K to 2100 K. This was explained by the fact that the usually dominating $\dot{Q}_{gas,red}$ and $\dot{Q}_{gas,ox}$ (see Fig. 4a and 5a) were significantly reduced and the energy balance was then dominated by the monotonically increasing $\dot{Q}_{heat\ loss}$. The solar-to-fuel

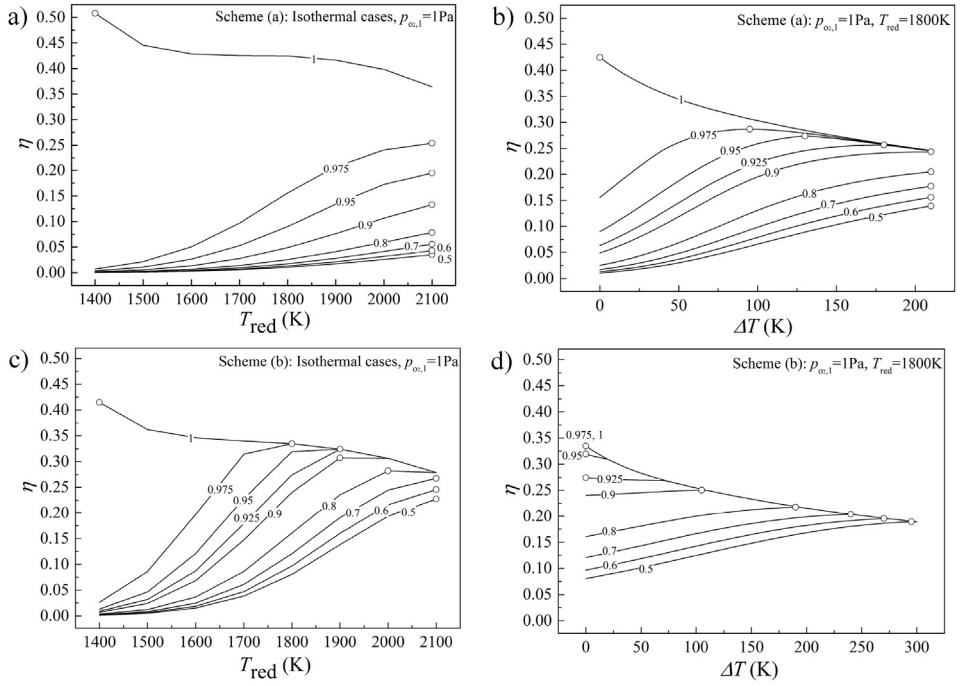

Fig. 9. Solar-to-fuel efficiency at isothermal conditions for $p_{O_2,1} = 1$ Pa and varying T_{red} and ε_g, for a) scheme (a), and c) scheme (b); and non-isothermal conditions at $p_{O_2,1} = 1$ Pa and $T_{red} = 1800$ K for varying ΔT and ε_g, for b) scheme (a), and d) scheme (b). The maximal efficiencies for each ε_g are marked by the dots.

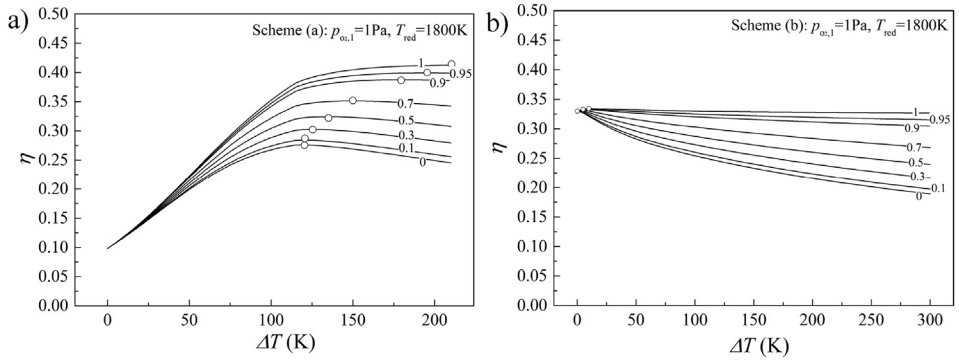

Fig. 10. Solar-to-fuel efficiency as a function of ΔT for varying ε_s at $p_{O_2,1} = 1$ Pa and $T_{red} = 1800$ K for a) scheme (a), and b) scheme (b). The maximal efficiencies for each ε_s are marked by the dots.

efficiency was significantly increased at perfect gas heat recovery: the solar-to-fuel efficiency increased up to 50% at $T_{red} = 1400$ K when ε_g increases from 0.975 to 1 for scheme (a). Similar behavior was observed for the non-isothermal operation of scheme (a) at $\varepsilon_g = 1$, namely solely a decrease in solar-to-fuel efficiency with increasing ΔT, which could again be explained by the reduction of the otherwise dominating $\dot{Q}_{gas,red}$ and $\dot{Q}_{gas,ox}$.

3.6.2. Solid phase heat recovery effectiveness

Effects of ε_s on η for varying ΔT are depicted in Fig. 10 at $T_{red} = 1800$ K and $p_{O_2,red} = 1$ Pa. Generally, η increased with increasing ε_s. This enhancement was more pronounced for larger ΔT due to the increased recuperation of $\dot{Q}_{solid}$. For scheme (a), a significant raise in the maximal optimal η of absolute 5% was observed when raising ε_s from 0 to 0.5. The optimal ΔT increased for maximal optimal η with increasing ε_s due to reduction in $\dot{Q}_{solid}$. $\dot{Q}_{solid}$ became less significant when ε_s increased above 0.5 and therefore the benefit of an increasing $\Delta\delta$ at higher ΔT dominated over the increased $\dot{Q}_{solid}$ and $\dot{Q}_{cool,ox}$.

As shown in Fig. 10b, scheme (b) displayed the maximal η at isothermal operation. η decreased with increasing ΔT at $\varepsilon_s < 0.9$ due to increase in $\dot{Q}_{solid}$ and $\dot{Q}_{cool,ox}$, which counteracted the decrease in $\dot{Q}_{pump}$ and increase in $\Delta\delta$. At $\varepsilon_s \geq 0.9$, a small ΔT of about 10 K led to increased η due to the increase of $\Delta\delta$ while the increase in $\dot{Q}_{cool,ox}$ and $\dot{Q}_{solid}$ were insignificant. As ΔT increased further, the benefit of increased $\Delta\delta$ became insignificant compared to the increasing losses.

3.7. Concentration ratio

The impact of concentration ratio, C, on η for schemes (a) and (b) is shown in Fig. 11. The C of a solar concentration system was determined by the type of the concentrator used and chosen from 1000 to 10,000 according to the feasibility of solar tower and dish systems [9].

Generally, higher C led to higher η, although the increase in η became small for $C > 5000$. For isothermal operation, η increased with T_{red} due to increasing $\Delta\delta$ and decreased due to the dominance

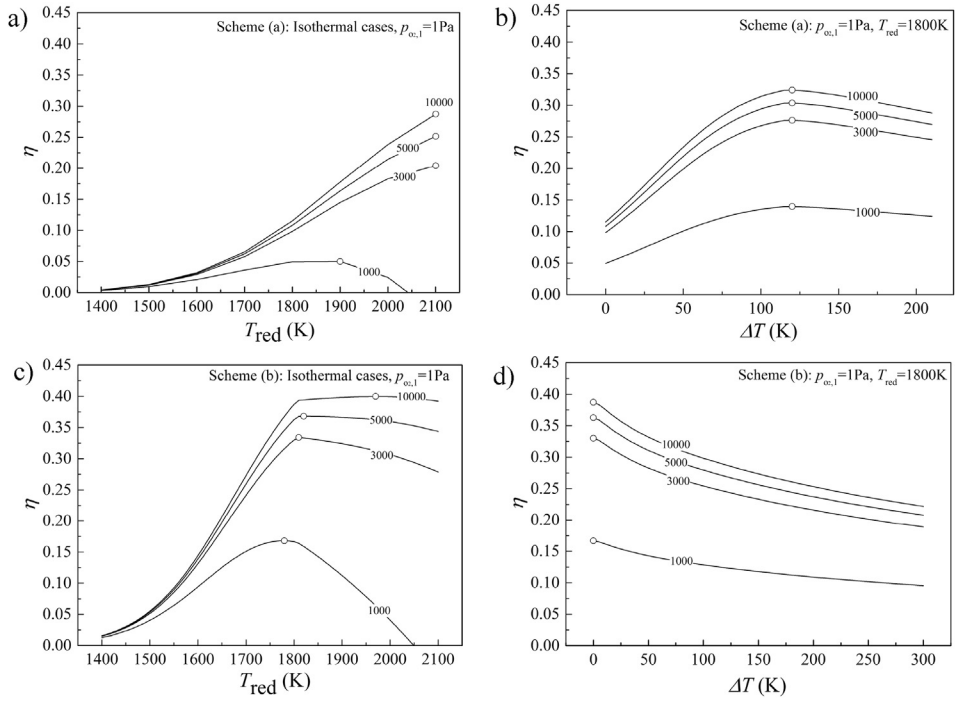

Fig. 11. η as a function of T_{red} for various C at $p_{O_2,1} = 1$ Pa at isothermal operation for a) scheme (a), and c) scheme (b). η as a function of ΔT for various C at $p_{O_2,1} = 1$ Pa and $T_{red} = 1800$ K for b) scheme (a), and d) scheme (b). The maximal efficiencies for each C are marked by the dots.

of $\dot{Q}_{\text{heat loss}}$ at high T_{red}. The decrease in η was reduced at increased C as the aperture was reduced and correspondingly the losses were relatively reduced (see eq. (5)). The optimal T_{red} for maximal η increased for the isothermal cases in schemes (a) and (b) due to the beneficial higher $\Delta\delta$. For the selected cases at $T_{\text{red}} = 1800$ K, the optimal ΔT for maximal optimal η was always at 120 K for scheme (a) and 0 K for scheme (b), respectively.

3.8. Reduction in the oxygen partial pressure through combined mechanical and mechanical-chemical approaches

Reduction in $p_{O_2,1}$ had the potential to significantly increase the solar-to-fuel efficiency. In order to further decrease the oxygen partial pressure while circumventing low pumping efficiencies, high pumping power requirements, or significant sensible heat losses required to heat the inert gas, a combination of mechanical and chemical techniques to reduce the oxygen partial pressure were proposed. Specifically, scheme (a) in combination with a chemical oxygen scavenger made of magnesium (scheme (c)) was investigated. The magnesium acted as reducing agent and reacts with the oxygen before it enters the reduction chamber. Magnesium is a strong reducing agent and is able to reduce the p_{O_2} in sweep gas to values lower than 10^{-17} atm [33]. The calculated efficiencies of scheme (c) under different $p_{O_2,1}$ are shown in Fig. 12a. The energy penalty introduced for MgO recycling was 3600 kJ/mol assuming MgO reduction by the Bolzano process [31]. The chemical reduction of $p_{O_2,1'}$ in the sweep gas led to higher η for the optimal cases because of a further reduction in the required sweep gas. For isothermal operation, the use of an oxygen scavenger showed no increase in η as the energy penalty caused by the large amount of magnesium required to scavenger the oxygen of the large amount of sweep gas traded off the increase in efficiency due by lower $p_{O_2,1}$.

The effect of $\dot{Q}_{\text{Mg,pr}}$ on the solar-to-fuel efficiency of the system is depicted in Fig. 12b and showed no significant efficiency penalty for the selected values of $\dot{Q}_{\text{Mg,pr}}$ between 0 and 9000 kJ/mol, which corresponded to free MgO recycling and MgO recycling by the Pidgeon process [31].

A combination of sweep gassing, vacuum pumping, and chemical scavenger (scheme e) allowed for a further increase in efficiency due to a decrease in system pressure. The basic idea of this combination was to reduce $p_{O_2,1}$ in the sweep gas from the baseline value (1 Pa), to a target value (0.1 Pa) through the oxygen scavenger. The vacuum pump was then used to further reduce the $p_{O_2,1}$ in reduction chamber by reducing the system pressure, p_{system}. Fig. 13 depicts the change of η with different p_{system} for both optimal and isothermal operations when varying p_{system} between 1 atm and 0.1 atm. For isothermal operation, we observed a minimum in η when decreasing p_{system} from 1 atm to 0.1 atm. The maximal η was

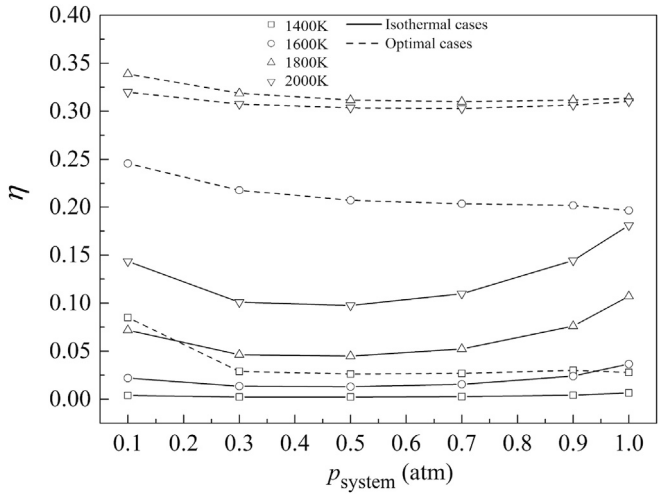

Fig. 13. η as a function of p_{system} for various T_{red} at $\dot{Q}_{\text{Mg,pr}} = 3600$ kJ/mol for both optimal and isothermal cases for scheme (c).

observed at $p_{\text{system}} = 1$ atm as the gain in efficiency with decreasing δ_{red} at low oxygen partial pressure was overruled by the large pumping work due to the large amount of sweep gas needed in isothermal operation.

For the optimal cases, a reduction in p_{system} increased the efficiency. This effect was less pronounced at higher temperatures as the amount of sweep gas required was higher at higher T_{red} which makes pumping work costly.

The use of vacuum pumping to lower the system pressure indicated less improvement in efficiency compared to the use of an oxygen scavenger in combination with sweep gassing (Fig. 12). This conclusion also held for the combination of the mechanical methods (sweep gassing + vacuum pumping, scheme (d)), where the same behavior as indicated in Fig. 13 was observed.

3.9. Counterflow versus ideal mixing reactor configurations

A counterflow arrangement represents a countercurrent flow between ceria and the gases which assumes that the gases are well mixed in the radial direction and only vary in the axial direction. The ideal mixing arrangement models a well-mixed reactor, resulting in no spatial variation of temperature, pressure, and species concentrations [34]. Compared to the counterflow arrangement, the ideal mixing arrangement required enormous amounts of sweep gas due to the need to maintain the whole reduction chamber at a low $p_{O_2,1}$. Owing to the large amount of

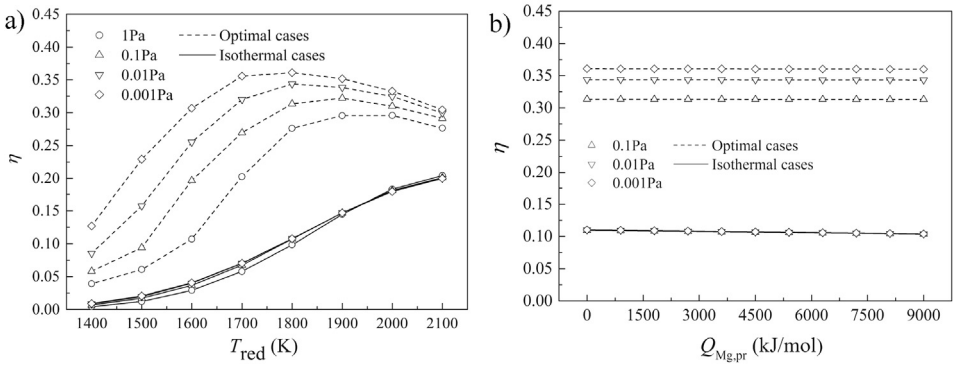

Fig. 12. a) η as a function of T_{red} at various $p_{O_2,1}$ for $\dot{Q}_{\text{Mg,pr}} = 3600$ kJ/mol for optimal and isothermal cases. b) η as a function of $\dot{Q}_{\text{Mg,pr}}$ for various of $p_{O_2,1}$ at $T_{\text{red}} = 1800$ K for optimal and isothermal cases.

sweep gas input, the previous studies utilizing ideal mixing arrangements [14,17] predicted that larger $p_{O_2,1}$ (of about 1000 Pa) favor larger efficiencies and operation at large ΔT (to ensure a complete oxidation of ceria).

The efficiencies of schemes (a) and (b) at various operating conditions for an ideal mixing arrangement are shown in Figs. S2 to S6. Scheme (a) always worked at low efficiencies ($\eta < 15\%$) and favored isothermal operation. The small efficiencies were caused by the large sweep gas and water input flow rates, respectively, which dominated the energy demand (Fig. S3). Scheme (b) showed efficiencies significantly larger than for scheme (a) due to a large decrease in the energy consumption to keep the $p_{O_2,1}$ in the reduction chamber low. Compared to the counterflow arrangement, the ideal mixing model tended to inefficiently use the water inflow and requires more sweep gas input, all of which led to significant lower efficiencies. The effect of changing ε_g on the system performance is shown in Fig. S5. As for the counterflow arrangement, for scheme (a) at isothermal conditions and in ideal mixing arrangement, larger ε_g resulted in larger efficiencies. This increase became more significant for $\varepsilon_g > 0.9$. Isothermal operation was favored in the ideal mixing arrangement as the reduction in $\dot{Q}_{gas,red}$ with increasing ΔT was to small to overcome the increase in $\dot{Q}_{ceria}$ and $\dot{Q}_{gas,ox}$ (Fig. S3c). Similar behavior in efficiency variation was observed for scheme (b) for the ideal mixing arrangement. However, scheme (b) could achieve larger efficiencies than scheme (a) as vacuum pumping required less energy than sweep gassing to maintain a low-oxygen atmosphere in the reaction chamber.

The influence of ε_s on the solar-to fuel efficiency is shown in Fig. S6a, and indicated negligible impact on scheme (a) in an ideal mixing arrangement due to the extremely low ceria flow rates. For scheme (b), the increase of ε_s led to higher efficiencies. However, this increase was small for large ΔT (Fig. S6b) due to the decreasing $\dot{Q}_{ceria}$ resulting from the decreasing ceria flow rate.

Generally, the ideal mixing arrangement is inferior to counterflow arrangement for schemes (a) and (b) because of significantly lower water utilization and the requirement of extremely large rates of sweep gas.

4. Summary and conclusions

A thermodynamic analysis was developed based on [13,14,17] to evaluate the solar fuel processing performance of a ceria-based thermochemical cycling scheme at various working conditions. Mechanical and chemical methods for the decrease of the oxygen partial pressure in the reduction chamber were proposed, compared, and combined. The impact of flow arrangement in the reactors (counterflow versus ideal mixing), temperature, pressure, solid and gas heat recovery effectiveness, and concentration ratio were discussed. Both isothermal and non-isothermal operation for ceria based redox cycles were studied to find the optimal configurations for best solar-to-fuel efficiency.

For the scheme using sweep gassing to reduce $p_{O_2,1}$ (scheme (a)), the non-isothermal operation predicted significant higher efficiency than isothermal operation even without solid phase heat recover. The optimal temperature difference between the reduction and oxidation temperature was in the range of 100 K–150 K and this slight temperature difference between reduction and oxidation reactions ensured a high solar-to-fuel efficiency trading off the energy consumption caused by solid phase heating and recycling of large amounts of sweep gas.

For the scheme using vacuum pumping to reduce $p_{O_2,1}$ (scheme (b)), the optimal efficiencies were obtained at isothermal operation, indicating a promising way to conduct isothermal operation bearing both high efficiency as well as simple design and operation. The efficiency of the vacuum pump was crucial in dictating a high efficiency and was predicted to be around 40% throughout the operational range.

The gas phase heat recovery significantly increased the efficiency for sweep gassing and vacuum pumping schemes. A minimum ε_g of 0.9 was required for efficiencies of 25% for both scheme (a) and scheme (b), working at conditions leading to the optimal efficiency. The requirement for ε_g could be relaxed by imposing a small ΔT (of around 100–200 K) with minimal efficiency reduction (below 3% when reducing ε_g from 0.975 to 0.9) for scheme (a) and scheme (b). The addition of solid phase heat recovery could further increase the efficiency. However, the absence of solid heat recovery didn't show a detrimental effect on the efficiency (efficiency reduction of 13.9% (scheme (a)) and 0.4% (scheme (b)) when changing ε_s from 1 to 0 at $T_{red} = 1800$ K and $p_{O_2,1} = 1$ Pa).

A high irradiation concentration led to lower radiation heat losses due to a reduced aperture area at the same solar energy input. The heat losses were dominating at large working temperatures due to the rapid increase of the radiation loss. The enhancement of the efficiency by increasing the concentration ratio became insignificant for concentrations above 5000.

A novel scheme combining mechanical approaches (sweep gassing) and chemical approaches (chemical scavenger) to reduce the oxygen partial pressures showed promise in further increasing the system efficiency at non-isothermal conditions. The energy penalty caused by using active metal was in a reasonable range (below 0.5% of input energy for optimal cases of scheme (c)) as the amount of required sweep gas was minimized at non-isothermal conditions. Consequently, the combination of sweep gassing with a chemical scavenger provided a significant jump in efficiency from 28% to 36% for optimal cases at 1800 K. For isothermal operation, the combined mechanical-chemical approach showed no enhancement effected by the large amount of required sweep gas. The combination of sweep gas, vacuum pumping, and a chemical oxygen scavenger could further improve the system efficiency, but less efficient as solely combining sweep gassing with an oxygen scavenger.

The counterflow and ideal mixing arrangement for fluid flow in reactor were implemented and compared. Generally speaking, the ideal mixing model is inferior to counterflow due to its inefficient use of sweep gas leading to extreme energy consumption in sweep gas heating, *i.e.* the maximum solar-to-fuel efficiency achieved for counter flow and ideal mixing arrangement was 18.2% and 4.3%, respectively, at $T_{red} = 1800$ K and $p_{O_2,1} = 10$Pa.

The developed thermodynamic model of ceria-based cycling for solar fuel processing offers guidelines for the design and operation of redox cycles for solar fuel processing and can straightforward be applied to other promising redox materials such as perovskites [35–37].

Acknowledgments

We acknowledge the funding from the European Union's Seventh Framework Programme (FP7/2007–2013) for the Fuel Cells and Hydrogen Joint Technology Initiative under grant agreement number 621173. We acknowledge the Chinese scholarship council for supporting Meng Lin's PhD work. We thank Roman Bader from the Australian National University for fruitful discussion of the thermodynamic model. We thank Stefan Brendelberger from the Deutsche Luft und Raumfahrt Zentrum for discussion about pump efficiencies.

Nomenclature

A	area (m^{-2})
c_p	specific heat capacity (J mol^{-1} K^{-1})

C	concentration ratio
G_0	direct normal irradiance (W m^{-2})
HHV	higher heating value (J mol^{-1})
χ_{H_2}	hydrogen productivity
f	heat loss factor
f_w	water utilization factor
h	molar enthalpy (J mol^{-1})
$\dot{n}$	molar flow rate (mol s^{-1})
p	pressure (Pa)
$\dot{Q}$	heat rate (W)
R	universal gas constant (8.3145 J mol^{-1} K^{-1})
T	temperature (K)
W	work rate (W)

Greek

Δg	Gibbs free energy of formation (J mol^{-1})
Δh	enthalpy of formation (J mol^{-1})
Δs	entropy of reaction (J mol^{-1} K^{-1})
$\Delta\delta$	non-stoichiometric coefficient difference
δ	non-stoichiometric coefficient
ε	heat recovery effectiveness
η	solar-to-fuel efficiency

Subscripts

0	ambient
1,2, …	state point
ap	aperture
cool	cooling
g	gas
in	inlet
Mg	magnesium
ox	oxidation
pump	pumping
pr	production
rad	radiation
red	reduction
react	reaction
scavenger	chemical scavenger

Appendix A. Supplementary data

Supplementary data related to this article can be found at http://dx.doi.org/10.1016/j.energy.2015.06.006.

References

[1] Steinfeld A. Solar thermochemical production of hydrogen––a review. Sol Energy 2005;78:603–15. http://dx.doi.org/10.1016/j.solener.2003.12.012.

[2] Bicakova O, Straka P. Production of hydrogen from renewable resources and its effectiveness. Int J Hydrogen Energy 2012;37:11563–78. http://dx.doi.org/10.1016/j.ijhydene.2012.05.047.

[3] Abanades S, Flamant G. Thermochemical hydrogen production from a two-step solar-driven water-splitting cycle based on cerium oxides. Sol Energy 2006;80:1611–23.

[4] Kodama T. High-temperature solar chemistry for converting solar heat to chemical fuels. Prog Energy Combust Sci 2003;29. http://dx.doi.org/10.1016/S0360-1285(03)00059-5.

[5] Perkins C, Weimer AW. Likely near-term solar-thermal water splitting technologies. Int J Hydrogen Energy 2004;29:1587–99. http://dx.doi.org/10.1016/j.ijhydene.2004.02.019.

[6] KOGAN A. Direct solar thermal splitting of water and on site separation of the products I. Theoretical evaluation of hydrogen yield. Int J Hydrogen Energy 1997;22:481–6. http://dx.doi.org/10.1016/S0360-3199(96)00125-5.

[7] Perkins C, Weimer AW. Solar-thermal production of renewable hydrogen. AIChE J 2009;55:286–93.

[8] Abanades S, Charvin P, Flamant G, Neveu P. Screening of water-splitting thermochemical cycles potentially attractive for hydrogen production by concentrated solar energy. Energy 2006;31:2469–86. http://dx.doi.org/10.1016/j.energy.2005.11.002.

[9] Kodama T, Gokon N. Thermochemical cycles for high-temperature solar hydrogen production. Chem Rev 2007;107:4048–77.

[10] Pregger T, Graf D, Krewitt W, Sattler C, Roeb M, Möller S. Prospects of solar thermal hydrogen production processes. Int J Hydrogen Energy 2009;34:4256–67. http://dx.doi.org/10.1016/j.ijhydene.2009.03.025.

[11] Siegel NP, Miller JE, Ermanoski I, Diver RB, Stechel EB. Factors affecting the efficiency of solar driven metal oxide thermochemical cycles. Ind Eng Chem Res 2013;52:3276–86.

[12] Chueh WC, Haile SM. A thermochemical study of ceria: exploiting an old material for new modes of energy conversion and CO_2 mitigation. Philos Trans R Soc A Math Phys Eng Sci 2010;368:3269–94. http://dx.doi.org/10.1098/rsta.2010.0114.

[13] Bader R, Venstrom LJ, Davidson JH, Lipiński W. Thermodynamic analysis of isothermal redox cycling of ceria for solar fuel production. Energy Fuels 2013;27:5533–44. http://dx.doi.org/10.1021/ef400132d.

[14] Lapp J, Davidson JH, Lipinski W, Lipiński W. Efficiency of two-step solar thermochemical non-stoichiometric redox cycles with heat recovery. Energy 2012;37:591–600. http://dx.doi.org/10.1016/j.energy.2011.10.045.

[15] Chueh WC, Haile SM. Ceria as a thermochemical reaction medium for selectively generating syngas or methane from H_2O and CO_2. ChemSusChem 2009;2:735–9.

[16] Hao Y, Yang C-K, Haile SM. High-temperature isothermal chemical cycling for solar-driven fuel production. Phys Chem Chem Phys 2013;15:17084–92.

[17] Ermanoski I, Siegel NP, Stechel EB. A new reactor concept for efficient solar-thermochemical fuel production. J Sol Energy Eng 2013;135:31002.

[18] Chueh WC, Falter C, Abbott M, Scipio D, Furler P, Haile SM, et al. High-flux solar-driven thermochemical dissociation of CO_2 and H_2O using non-stoichiometric ceria. Science 2010;330:1797–801. http://dx.doi.org/10.1126/science.1197834.

[19] Furler P, Sche J, Gorbar M, Moes L, Vogt U, Steinfeld A. Solar thermochemical CO_2 splitting utilizing a reticulated porous ceria redox system. 2012.

[20] Furler P, Scheffe J, Marxer D, Gorbar M, Bonk A, Vogt U, et al. Thermochemical CO_2 splitting via redox cycling of ceria reticulated foam structures with dual-scale porosities. Phys Chem Chem Phys 2014;16:10503–11.

[21] Furler P, Scheffe JR, Steinfeld A. Syngas production by simultaneous splitting of H_2O and CO_2 via ceria redox reactions in a high-temperature solar reactor. Energy Environ Sci 2012;5:6098–103.

[22] Roeb M, Sattler C. Isothermal water splitting. Sci (80-) 2013;341:470–1. http://dx.doi.org/10.1126/science.1241311.

[23] Muhich CL, Evanko BW, Weston KC, Lichty P, Liang XH, Martinek J, et al. Efficient generation of H-2 by splitting water with an isothermal redox cycle. Sci (80-) 2013;341:540–2. http://dx.doi.org/10.1126/science.1239454.

[24] Lundberg M. Model calculations on some feasible two-step water splitting processes. Int J Hydrogen Energy 1993;18:369–76.

[25] Panlener RJ, Blumenthal RN, Garnier JE. A thermodynamic study of non-stoichiometric cerium dioxide. J Phys Chem Solids 1975;36:1213–22.

[26] Riess I, Ricken M. On the specific heat of nonstoichiometric ceria. J Solid State Chem 1985;57:314–22.

[27] Pai BC, Ramani G, Pillai RM, Satyanaryana KG. Role of magnesium in cast aluminium alloy matrix composites. J Mater Sci 1995;30:1903–11.

[28] Dulski TR. Trace elemental analysis of metals: methods and techniques. CRC Press; 1999.

[29] Wulandari W, Brooks GA, Rhamdhani MA, Monaghan BJ. Magnesium: current and alternative production routes. In: Chemeca 2010 Eng Edge; 26–29 Sept 2010, Hilt Adelaide, South Aust; 2008. p. 347.

[30] Charvin P, Stéphane A, Florent L, Gilles F. Analysis of solar chemical processes for hydrogen production from water splitting thermochemical cycles. Energy Convers Manag 2008;49:1547–56. http://dx.doi.org/10.1016/j.enconman.2007.12.011.

[31] Cherubini F, Raugei M, Ulgiati S. LCA of magnesium production. Resour Conserv Recycl 2008;52:1093–100. http://dx.doi.org/10.1016/j.resconrec.2008.05.001.

[32] Brendelberger S, Sattler C. Concept analysis of an indirect particle-based redox process for solar-driven H_2O/CO_2 splitting. Sol Energy 2015;113:158–70. http://dx.doi.org/10.1016/j.solener.2014.12.035.

[33] Gratz ES, Guan X, Milshtein JD, Pal UB, Powell AC. Mitigating electronic current in molten flux for the magnesium SOM process. Metall Mater Trans B 2014;45:1–12. http://dx.doi.org/10.1007/s11663-014-0060-9.

[34] Rawlings JB, Ekerdt JG. Chemical reactor analysis and design fundamentals. Nob Hill Pub, Llc; 2002.

[35] Yang C-K, Yamazaki Y, Aydin A, Haile SM. Thermodynamic and kinetic assessments of strontium-doped lanthanum manganite perovskites for two-step thermochemical water splitting. J Mater Chem A 2014;2:13612. http://dx.doi.org/10.1039/C4TA02694B.

[36] Nalbandian L, Evdou A, Zaspalis V. La1−xSrxMO3 (M = Mn, Fe) perovskites as materials for thermochemical hydrogen production in conventional and membrane reactors. Int J Hydrogen Energy 2009;34:7162–72. http://dx.doi.org/10.1016/j.ijhydene.2009.06.076.

[37] Evdou a, Nalbandian L, Zaspalis VT. Perovskite membrane reactor for continuous and isothermal redox hydrogen production from the dissociation of water. J Memb Sci 2008;325:704–11. http://dx.doi.org/10.1016/j.memsci.2008.08.042.